# RhoB-dependent modulation of postendocytic traffic in polarized Madin-Darby canine kidney cells

Christine Rondanino[‡1], Raul Rojas[‡1,2], Wily G. Ruiz[‡], Exing Wang[¶], Rebecca P. Hughey[‡], Kenneth W. Dunn[¶], and Gerard Apodaca[‡§3]

[‡]Laboratory of Epithelial Biology/Renal-Electrolyte Division of the Department of Medicine, and [§]Department of Cell Biology and Physiology, University of Pittsburgh, Pittsburgh, PA 15261, and [¶]Department of Medicine, Division of Nephrology, Indiana University Medical Center, Indianapolis, IN 46202, USA

Running title: RhoB and early endocytic traffic

[1]These authors contributed equally to this work

[2]Current address: Cell Biology and Metabolism Branch, National Institute of Child Health and Human Development, Bethesda, MA 20892

[3]Address correspondence to: Gerard Apodaca, Ph.D., University of Pittsburgh, Renal Division, 982 Scaife Hall, 3550 Terrace Street, Pittsburgh, PA 15261, Tel. 412 383-8893; Fax. 412 383-8955/8956; E-mail: gla6@pitt.edu

**The Rho-family of GTPases is implicated in the control of endocytic and biosynthetic traffic of many cell types; however, the cellular distribution of RhoB remains controversial and its function is not well understood. Using confocal microscopy we found that endogenous RhoB and green fluorescent protein tagged-wild-type RhoB were localized to early endosomes, and to a much lesser extent to recycling endosomes, late endosomes, or Golgi complex of fixed or live polarized Madin-Darby canine kidney cells. Consistent with RhoB localization to early endosomes, we observed that expression of dominant negative RhoBN19 or dominant active RhoBV14 altered postendocytic traffic of ligand-receptor complexes that undergo recycling, degradation, or transcytosis. *In vitro* assays established that RhoB modulated the basolateral-to-apical transcytotic pathway by regulating cargo exit from basolateral early endosomes. Our results indicate that RhoB is localized, in part, to early endosomes where it regulates receptor egress through the early endocytic system.**

The Rho family of small GTPases is a large family of proteins that couple extracellular signaling events to changes in cellular function. They act as molecular switches that can cycle between a cytoplasmic GDP-form ("off" state) and a membrane-bound GTP form ("on" state). In their GTP-bound state Rho GTPases bind effector molecules, generating cellular responses that are terminated upon GTP hydrolysis. In addition to regulating the actin cytoskeleton, Rho GTPases are known to control diverse cellular events including apoptosis, cell motility, cell growth, development, gene expression, and progression through the cell cycle (1). In addition, there is mounting evidence that some Rho family members (e.g., Cdc42, Rac1, RhoA, RhoD, and TC10) are important regulators of various membrane trafficking events including endocytosis and transport of internalized cargo within the endosomal system (2).

RhoB, a protein that is 92% homologous to the well-characterized RhoA protein, was originally shown to be associated with endosomes (3), but there remains significant controversy concerning the specific intracellular compartments to which it associates. Endogenous RhoB has been

localized to late endosomal/lysosomal compartments (4,5), while overexpressed myc-tagged wild-type RhoB (RhoBWT) is reported to be associated with early endosomes and other uncharacterized endosomal compartments (3,6,7). A GTPase-deficient mutant of RhoB, RhoBV14, is variously localized to the plasma membrane, early endosomes (7), and multivesicular compartments, possibly late endosomes (8). In contrast, studies using green fluorescent protein (GFP)-tagged RhoB indicate that in unfixed MDCK[4] cells the GTPase is excluded from endosomes and instead localizes to the Golgi, peri-Golgi vesicles, and plasma membrane (9). In other studies RhoB has been localized to the nuclear membrane (10).

Consistent with its endosomal distribution, there are several reports that RhoB regulates traffic in the endocytic system. Overexpression of RhoBWT or expression of a dominant active mutant of RhoB (RhoBQ63L) slows the transit of receptor-bound EGF between endocytic compartments, in a process that may involve the PKC-related protein 1 (PRK1) (11,12). More recent analysis indicates that RhoB modulates transit of EGF between late endosomes and lysosomes, a function ascribed to geranylgeranylated but not farnesylated forms of RhoB (2,4). However, expression of dominant-negative RhoBN19, which should prevent activation of endogenous RhoB, has no effect on EGF degradation (12). Other studies demonstrate that expression of dominant-active RhoBV14 slows endosome movements and function, a likely consequence of Diaphanous-related formin Dia1-dependent actin polymerization around endosomes (7). While a dominant negative mutant of Dia1 (Dia1-N1) inhibits RhoBV14-dependent effects on endosome dynamics, Dia1-N1 apparently has no effect when expressed in the absence of RhoBV14. Thus, the regulation of endosome dynamics by Dia1 and endogenous RhoB remains an open question. Other studies point to a role of RhoB in regulating Src activation (6), which depends on RhoB-dependent actin polymerization and endosomal traffic, and in mannose receptor-mediated phagocytosis by macrophages (13).

At present there is little understanding of RhoB function in polarized epithelial cells. These cells have discrete apical and basolateral plasma membrane domains and associated endocytic trafficking pathways including a tissue-specific transcytotic pathway that allows for transport between the two epithelial cell plasma membrane domains. The goals of this analysis were twofold: (*i*) to define the intracellular compartments to which endogenous RhoB was localized in polarized Madin-Darby canine kidney (MDCK) cells; and (*ii*) to determine which endocytic trafficking steps, if any, were modulated by RhoB. Using quantitative and qualitative microscopy we observed that endogenous RhoB was associated, in part, to early endosomes, and to a much lesser extent to recycling endosomes, late endosomes and the Golgi complex. Consistent with its location to early endosomes, we observed that expression of RhoBN19 or RhoBV14 impaired the transport of various ligands whose initial itinerary involves passage through early endosomes including basolateral recycling of transferrin (Tf), EGF degradation, apical recycling of IgA, and basolateral-to-apical transcytosis of IgA. Additional study established that RhoB modulates IgA exit from basolateral early endosomes, further defining a specific event regulated by RhoB in the cell.

## EXPERIMENTAL PROCEDURES

*Antibodies* - Mouse anti-myc monoclonal antibody 9E10 hybridoma supernatant (hybridoma cell line provided by Dr. S.W. Whiteheart, University of Kentucky, Lexington, KY) was used at 1:20 dilution, while affinity purified mouse monoclonal anti-myc 9E10 antibodies (Covance, Princeton, NJ) were used at 1:1000 dilution; affinity-purified rabbit polyclonal anti-cation independent mannose-6-phophate receptor (M6PR) (Dr. Linton Traub, University of Pittsburgh, Pittsburgh, PA) was used at 6 μg/ml; rabbit polyclonal anti-early endosome antigen 1 (EEA1) antibody (Dr. S. Corvera, University of Massachusetts Medical School, Worcester, MA) was used at 1:250; rabbit polyclonal anti-giantin serum (Dr. Adam Linstedt, Carnegie Mellon University, Pittsburgh, PA) (14) was used at a dilution of 1:250; affinity-purified rabbit polyclonal anti-human IgA antibody (Jackson Immunoresearch Laboratories, West Grove, PA) was used at 24 μg/ml; rabbit anti-myc polyclonal antibody (Cell Signaling, Beverly, MA) was used at 2 μg/ml; rabbit polyclonal anti-Rab11 serum (kindly provided by Dr. Jim Goldenring, Vanderbilt University, Nashville, TN) was used at

a 1:500 dilution; purified mouse anti-RhoB monoclonal antibody (Santa Cruz Biotechnology Inc., Santa Cruz, CA) was used at 2 µg/ml; rabbit polyclonal anti-canine Tf serum (15) was used at 1:100 dilution; rabbit polyclonal anti-actin (Abcam, Cambridge, UK) was used at a 1:100 dilution; affinity-purified and minimal cross reacting Alexa-488-conjugated secondary antibodies (Molecular Probes, Eugene, OR) were used at 4 µg/ml and affinity-purified and minimal cross reacting FITC- and Cy5-conjugated secondary antibodies (Jackson Immunoresearch Laboratories) were used at 6 µg/ml; goat-anti-mouse antibody conjugated to HRP (Kirkegaard and Perry Laboratories, Gaithersburg, MD) was used at 0.4 µg/ml and goat-anti-mouse antibody conjugated to HRP (Jackson Immunoresearch Laboratories) was used at 50 ng/ml; human polymeric IgA was purchased from Dr. J.-P. Vaerman, Catholic University of Louvain, Belgium and used at 0.2 mg/ml.

*DNA cloning and generation of cell lines* - The cDNA encoding RhoBWT containing an N-terminal c-Myc epitope tag was amplified by PCR from the plasmid pEGFP-Endo (Clontech, Palo Alto, CA). The fragment was digested with BamHI and SalI, and then inserted into the pTRE2hyg vector that carries a hygromycin B selection marker (Clontech), generating pTRE2hyg-RhoBWT. RhoBV14 was engineered by using the Quickchange site-directed mutagenesis kit (Stratagene, La Jolla, CA) to change Gln-14 to Val, while RhoBN19 was generated by changing Thr-19 to Asn. The identity of all constructs was confirmed by nucleotide sequencing.

MDCK cells stably expressing RhoBWT or RhoB mutants were created using a tetracycline-repressible system as described previously (16). In brief, parental MDCK cells II (T23 clone), which express a tetracycline-regulated transactivator and the pIgR, were transfected using Transfectol (Gene Choice, Frederick, MD) with pTRE2hyg-RhoBWT, pTRE2hyg-RhoBV14 or pTRE2hyg-RhoBN19. The transfected cells were selected in the presence of 250 µg/ml hygromycin B and doxycycline (DC). We used 100 ng/ml DC to repress RhoBN19 expression. However, in preliminary experiments we observed that expression of RhoBV14 and RhoBWT was leaky, so the concentration of DC was raised to 200 ng/ml for RhoBV14 cells and 300 ng/ml for RhoBWT cells. Following 14 d in selection medium, surviving clones were picked. Screening was performed on cells that were grown in the absence of DC and expression of RhoBWT and RhoB mutant proteins was assessed by immunoblotting or immunofluorescence microscopy using a monoclonal antibody specific for the myc epitope tag (9E10). Positive clones were expanded in the presence of DC, divided into aliquots, and stored in liquid nitrogen. Several clones were screened for polarized secretion of gp-80 (17) and a transepithelial resistance of >120 $\Omega*cm^2$ when cultured on Transwells (Corning-Costar Corp., Cambridge, MA) in the presence of DC. The data presented are from an individual, representative clone that uniformly expressed either myc-RhoBWT or myc-RhoB mutant when cells were cultured in the absence of DC. However, similar results were obtained with other clones expressing these mutant proteins.

To generate MDCK cells expressing GFP-RhoB, MDCK cells expressing the pIgR under control of a plasmid encoding hygromycin resistance (A4 cells) were transfected with pEGFP-Endo using $Ca_2(PO_4)_3$-precipitation. The transfected cells were selected in the presence of 800 µg/ml of G-418 for 14 days before surviving colonies were picked. Clones were selected that showed positive expression for GFP-RhoB by fluorescence microscopy and by immunoblotting and immunofluorescence microscopy using a monoclonal antibody specific for the myc-epitope tag (9E10).

*Cell culture and induction of wild-type and mutant RhoB, and RhoAN19 expression* - The cell lines were routinely cultured in MEM (Cellgro, Herndon, VA) containing 10% (v/v) FBS (Hyclone, Logan, UT), 1% (v/v) penicillin/streptomycin, and 0-300 ng/ml of DC at 37˚ C in a humidified atmosphere containing 5% $CO_2$. Expression of RhoBWT or RhoB mutants was induced by plating cells on 15 cm dishes at low density into MEM/FBS medium in the absence of DC and incubating them for 24 h at 37°C. At the end of this incubation period, the cells had reached ~25% confluence. Cells treated in an identical manner, but in the presence of DC, served as controls. The cells were detached with

trypsin/EDTA and washed with MEM/FBS. Next, 1 x $10^6$ cells (resuspended in MEM/FBS±DC) were added to the apical chamber of rat tail collagen-coated, 12-mm-diameter Transwells. Cells were incubated in MEM/FBS ± DC for 24-48 h. GFP-RhoB expressing cells were cultured on rat tail collagen-coated Transwells in MEM medium containing 10% (v/v) FBS, 1% penicillin/streptomycin, at 37˚C in a humidified atmosphere containing 5% $CO_2$, and were used 2-3 days post-plating. Cells expressing RhoAN19 were cultured as described previously (18). Control experiments confirmed that concentrations of DC up to 300 ng/ml had little effect on the endocytic trafficking steps we measured.

*Immunoprecipitation of endogenous RhoB and western blot analysis* - MDCK cells expressing mutant RhoB were grown on 75-mm-diameter Transwells in the presence or absence of DC as described above. For immunoprecipitation of endogenous and mutant RhoB, cells were metabolically labeled for 4 h at 37˚C with 0.05 mCi/ml of [$^{35}$S]methionine/cysteine (Express Protein Label, Dupont-New England, Boston, MA) in methionine/cysteine-free DMEM supplemented with 10% dialyzed fetal bovine serum. After labeling, cells were washed twice with ice-cold PBS, scraped into 5 ml of ice-cold PBS, and collected by centrifugation at 175 x *g*. The cell pellet was resuspended in 200 µl of fresh PBS and the suspension was transferred into a centrifuge tube kept on ice. Cells were solubilized at room temperature by adding 1 ml of HEPES-buffered saline (HBS, 10 mM HEPES-NaOH pH 7.4, 150 mM NaCl) containing 60 mM n-octyl-ß-D-glucopyranoside, 0.1% (w/v) SDS, and a protease inhibitor cocktail (Roche, Indianapolis, IN) for 30 min. Insoluble material was removed by centrifugation in a microcentrifuge at 14,000 x *g* for 15 min at 4˚C. Supernatants were recovered and rotated end-over-end overnight at 4˚C after addition of mouse monoclonal anti-RhoB antibody and protein G conjugated to Sepharose (Amersham Pharmacia Biotech, Piscataway, NJ). Immunoprecipitates were recovered by brief centrifugation and washed once with 0.5 ml of the following: 1% (v/v) Triton X-100 in HBS, 0.01% (w/v) SDS in HBS, and finally HBS. Proteins were recovered by heating for 5 min at 90˚C in 50 µl of NuPAGE-sample buffer (Invitrogen) containing fresh 0.14 M ß-mercaptoethanol. Samples were subjected to SDS-PAGE on 4-12% acrylamide gradient gels and $^{35}$S-labeled protein detected by fluorography.

For detection of myc-tagged wild-type and mutant RhoB present in cell homogenates, lysates were resolved by SDS-PAGE, proteins were transferred to nitrocellulose membranes, and then blocked with 5% BSA/PBS. The nitrocellulose membranes were incubated with affinity purified mouse anti-myc 9E10 antibody at 1:1000 dilution for 2 h followed by 1 h incubation with donkey-anti-mouse antibody conjugated to HRP. The secondary antibodies were detected by chemiluminescence (NEN). Quantification of the levels of expression of mutant RhoB relative to endogenous RhoB was done using a Phosphoimager (Molecular Dynamics) and the Image Quant v5.2 software (Molecular Dynamics).

*Immunofluorescent labeling and scanning-laser confocal microscopy* - In most experiments cells were fixed and processed using a pH-shift protocol as previously described (15) and permeabilization was effected by addition of 0.025% (w/v) saponin during the blocking step. The localization of endogenous RhoB was performed as follows. Filter-grown MDCK cells expressing pIgR (19) were washed with phosphate buffered saline (PBS) and fixed for 10 min with 4% (w/v) paraformaldehyde in PBS at room temperature. The cells were rinsed twice with PBS: excess paraformaldehyde was quenched with PBS containing 20 mM glycine pH 8.0 and 75 mM $NH_4Cl$ for 15 min at room temperature, the cells were again washed with PBS and permeabilized with 0.025% (w/v) saponin prepared in block solution (PBS containing 5% [v/v] goat serum and 8.5 mg/ml of fish skin gelatin) for 10 min at 37˚C in a humid chamber. Cells were immunostained with appropriate antibodies overnight at 4˚C, followed by incubation with fluorescent-labeled secondary antibodies. For the actin cytoskeleton staining, rhodamine-labeled phalloidin (Molecular Probes, Eugene, OR) was added at a 1:100 dilution during the incubation with the secondary antibodies. Alternatively, actin was stained using an anti-actin antibody (Abcam, Cambridge, UK) in cells fixed with 100% methanol for 10 min at -20˚ C. When examining the distribution of

endogenous RhoB we observed staining when 0.025% saponin was used to permeabilize the cells; however, permeabilization with 0.1% Triton X-100 resulted in a significantly diminished RhoB signal. Imaging was performed on a TCS-SL confocal microscope (Leica, Dearfield, IL) equipped with argon, green helium-neon and red helium-neon lasers. Images were acquired using a 100x plan-apochromat oil objective (NA 1.4) and the appropriate filter combination. Settings were as follows: photomultipliers set to 600-800 V, Airy = 1, zoom = 2.0-3.0, Kalman filter (n = 4). The images (512 x 512 pixels) were saved in a tag-information-file-format (TIFF), contrast was corrected in Photoshop (Adobe, San Jose, CA), and the images were imported in Freehand 11.0 (Macromedia, San Francisco, CA).

*Imaging processing, quantification of colocalization, and live-cell imaging* - Colocalization was measured using Metamorph v. 5.0 (Universal Imaging, Downingtown, PA) software. Confocal Z-series of double-labeled cells were stacked, smoothed by a 3x3 low pass filter, and background corrected by subtracting 32 x 32 median filtered images (20). A mask (as a binary image-stack) for punctate objects was created by thresholding the background corrected images. The background corrected image-stack from channel A (RhoB) was combined with the mask for channel A (plane by plane), using a logical "AND" operation, to produce an image-stack with only punctate structures (stack1). The background corrected image-stack from channel A was combined with the mask for channel B (Tf, M6PR or giantin) to produce an image-stack containing the punctate fluorescence of channel A that colocalized with punctate fluorescence of channel B (stack2). The integrated fluorescence intensities of the two stacks, sum1 and sum2 (for stack1 and stack2 respectively), were then calculated using stack arithmetic. The ratio of the two, sum1/sum2, represented the fraction of punctate objects in channel A that colocalized with punctate objects in channel B. Cells in which one of the two proteins were not expressed or contained saturated pixels were excluded from analysis. Alternatively, confocal image stacks were imported into the Volocity program (Improvision, Lexington, MA). The labeled objects in each channel were chosen using the classifier function and the degree of overlap in the total image volume was measured using session arithmetic and the colocalization function. The percent of colocalization was measured by taking the volume of RhoB signal that overlapped with the protein marker in the other channel and dividing it by the total volume of RhoB in the sample.

For live-cell imaging, MDCK cells stably expressing GFP-RhoB were cultured on 24-mm Transwell filters for 2-3 days. The cells were rinsed twice with MEM/BSA (MEM containing 2.5 g/l $NaHCO_3$, 20 mM HEPES, pH 7.4, 0.6% [w/v] bovine serum albumin) at 37˚C. To label early endosomes, the fluid-phase marker Alexa-546-dextran (Molecular Probes, Eugene, OR), final concentration of 5 mg/ml in MEM/BSA, was internalized from the basolateral (or apical) surface of the cells for 5 min in a humid chamber. The cells were then washed three times for 10 min with ice-cold MEM/BSA. To label late endosomes, the fluid-phase marker was internalized for 5 min at 37˚C, washed with ice-cold MEM/BSA three times for 10 min, and chased in MEM/BSA at 37˚C for 40 min. Prior to visualization, cells were quickly washed twice with MEM/BSA and the filter assembly was placed into a Mat-Tek dish (Mat-Tek Corporation, Ashland, MA) positioned on the stage of the Leica TCS-SL confocal microscope equipped with a HCX APO LU-V-I 63x water immersion objective (NA 0.9) and the appropriate filter combination. The washing/mounting steps and acquisition of the images took less than 3 min.

To label the Golgi complex, GFP-RhoB expressing cells were washed twice with 20˚C P-buffer (20 mM HEPES, pH 7.4, 2 mM sodium pyruvate, 20 mM glucose, 6 mM $CaCl_2$ and 290 mM NaCl), incubated at 18.5˚C for 10 min, and then 0.5 ml of 0.5 μM BODIPY-Ceramide-Texas Red (Molecular Probes, Eugene, OR), complexed to defatted-BSA (Boehringer Mannheim Corp, Indianapolis, IN) as described previously (16), was added to the apical surface of the cells for 60 min at 20˚C. P-buffer (1 ml) containing 0.34 mg/ml defatted-BSA was added to the basolateral surface. The apical and basolateral media were aspirated and fresh P-buffer containing 1% (w/v) defatted-BSA was added for 60 min at 20˚C. This step was repeated one additional time. Cells were washed twice with 20˚C P-buffer, the filter was quickly cut out the holder, mounted under a coverslip, and

immediately imaged at room temperature with a Fluoview-BX61 confocal microscope (Olympus, Melville, NY) using a 100x plan-apochromat objective (NA 1.4) and the appropriate filter combination. Mounting and imaging collection took approximately 3-5 min to complete.

*Measurement of transepithelial resistance and paracellular diffusion of [$^{125}$I]IgA, and [$^{125}$I]Tf* - Transepithelial resistance and paracellular diffusion of [$^{125}$I]IgA and [$^{125}$I]Tf were measured as described previously (16).

*Endocytosis of [$^{125}$I]IgA and analysis of postendocytotic fate of [$^{125}$I]IgA, [$^{125}$I]Tf, and [$^{125}$I]EGF* - Endocytosis of [$^{125}$I]IgA and postendocytotic fate of [$^{125}$I]IgA, [$^{125}$I]Tf, and [$^{125}$I]EGF were performed as described previously (15,18,21).

*Diaminobenzidine density-shift assay* - The diaminobenzidine density-shift assay was performed as described previously (18). Values were normalized to reactions in which [$^{125}$I]IgA and wheat germ agglutinin (WGA) conjugated to horseradish peroxidase (HRP) were co-internalized from the apical pole of the cell. In initial control experiments, we confirmed that endocytosis of WGA-HRP from the apical surface of RhoBV14 and RhoBN19 was not altered by RhoB mutant expression.

*Preparation of cytosol* - Cytosol was prepared as described by Bomsel *et al.* (22) with the following modifications. Cells, grown in the presence or absence of DC, were plated at 60-75% confluency on twenty 15-cm diameter cell culture dishes and then incubated for one day. All subsequent steps were performed at 4˚C. Cells were washed twice with ice-cold PBS, the cells were detached with trypsin/EDTA. After three washes with MEM/FBS and three washes with PBS, cells were centrifuged at 100 x g for 10 min. The cell pellet was resuspended in homogenization buffer (HB) composed of 10 mM HEPES pH 7.4, 250 mM sucrose, 0.5 mM EDTA, containing 1 mM dithiothreitol (DTT), 1 mM phenylmethylsulphonylfluoride (PMSF) and a protease inhibitor cocktail (comprised of 5 µg/ml each of pepstatin, leupeptin, and antipain) and homogenized by passing the cells through a Rainin Pipetman bluetip 20 times followed by 10 passages through a 22G 1-and-1/2-inch-long needle. The homogenate was centrifuged at 10,000 x g for 10 min, and the resulting supernatant was centrifuged at 100,000 x g for 30 min. The supernatant of the high-speed centrifugation, corresponding to the cytosol fraction (4-5 mg/ml), was collected and immediately used in the assay, or aliquoted, flash-frozen in liquid nitrogen, and stored at –80˚C. Expression of RhoBV14 or RhoBN19 in membrane and cytosolic fractions was detected by western blot analysis as described previously (21).

*IgA vesicle release assay* - Reconstitution of vesicle-release from early endosomes was performed as described previously (23) with the following modification: cytosol (2 mg/ml final concentration) was from control cells (+DC) or from cells expressing mutant RhoB or RhoAN19.

*F-actin analysis* - MDCK cells expressing mutant RhoB were grown on 75-mm-diameter Transwells ± DC. Extraction of the Triton-insoluble and the Triton-soluble pools of actin was performed as described previously (24). Briefly, cells were rinsed with PBS and the Triton-soluble fraction extracted by incubating the cells for 5 min at room temperature with 0.5 ml of 50 mM 2-(*N*-morpholino)ethanesulfonic acid pH 6.5, 1 mM EGTA, 50 mM KCl, 1 mM $MgCl_2$, 1 mM phenylmethylsulfonyl fluoride, 10 mM NaF, 0.5% Triton X-100, and a protease inhibitor cocktail (comprised of 5 µg/ml each of pepstatin, leupeptin, and antipain). The Triton-soluble material was transferred to a microcentrifuge tube containing 50 µl of 20% SDS and boiled for 5 min. The remaining Triton-insoluble cytoskeletal fraction was further solubilized in 0.5 ml of 50 mM triethanolamine, pH 8.6, 100 mM NaCl, 5 mM EDTA, 0.5% SDS, recovered from the surface of the filter with a cell scraper and then transferred to a microcentrifuge tube, boiled for 5 min, and vortex-shaken for 15 min at 4°C. Protein content was assessed using the BCA protein assay kit as described by the manufacturer (Pierce, Rockford, IL). BSA was used as the standard. For western blot, 15 µg of protein/fraction were loaded.

## RESULTS

*RhoB is localized to the early endosomes of polarized MDCK cells* - Because expression of wild-type, mutant, or tagged RhoB may significantly impact the intracellular traffic and thus the distribution of these and other marker proteins, we first examined the localization of endogenous RhoB by immunofluorescence. In polarized MDCK cells, endogenous RhoB was found at or near the basolateral plasma membrane and also in a population of small vesicular structures that were positioned along the basolateral surface and in the apical cytoplasm (Figure 1A-C). No staining was observed when competing antigenic peptide was added during the primary antibody incubation (our unpublished observations).

To determine the nature of the RhoB-associated vesicular structures, we first co-stained cells with RhoB specific antibodies and antibodies against the following proteins: Tf, a marker of basolateral early endosomes and recycling endosomes (25); giantin, a marker of the Golgi (14); or the M6PR, a protein found predominantly in late endosomes and the *trans*-Golgi network (TGN) (26). Two-color confocal images were collected through the whole cell volume and the extent of overlap of vesicular structures between the two channels was quantified by computational analysis (see Experimental Procedures). RhoB colocalized in part with Tf-positive endosomes (31.0 ± 3.0%; Figure 1D-F), but colocalization between RhoB and M6PR-labeled compartments (Figure 1G-I) or giantin-labeled membranes (Figure 1J-L) was significantly less, 7.0 ± 0.5% and 4.0 ± 0.5%, respectively.

Additional experiments were performed to further delineate the compartments to which RhoB is associated. We observed that 23.2 ± 2.0% of endogenous RhoB colocalized with the early endosomal marker EEA1 (27), indicating partial association of RhoB with early endosomes (Figure 2A-F). There was limited colocalization between endogenous RhoB and Rab11 (1.1 ± 0.4%), which labels apical recycling endosomes (Figure 2G-I) (28,29). To further confirm that there was little colocalization between endogenous RhoB and late endosomes, we compared the distribution of RhoB and dextran, internalized for 10 min at 37ºC followed by a 30 min incubation to chase the marker into late endosomes (30). Little observable colocalization was observed under these conditions (our unpublished observations). In addition, furin, which is localized to the TGN at steady state, showed little colocalization with endogenous RhoB (our unpublished observations). These results indicate that endogenous RhoB is localized in part to the early endosomes, and to a much lesser degree with late endosomes, recycling endosomes, the Golgi complex, or the TGN of polarized MDCK cells.

*GFP-RhoB is also associated with early endosomes in living cells* - It was previously reported that the distribution of RhoB may be altered by fixation (9). To confirm if the distribution of RhoB we observed in fixed and permeabilized cells reflects its distribution in living polarized MDCK cells, we generated an MDCK cell line that stably expressed a chimeric protein containing GFP fused to the N-terminus of myc-tagged RhoB (GFP-RhoB). Using quantitative immunoblotting it was observed that GFP-RhoB was expressed at levels ~10 fold above endogenous RhoB (data not shown). In unfixed cells GFP-RhoB was localized, like endogenous RhoB, to the basolateral surface of the cell and to vesicular structures that were found near the basolateral plasma membrane and in the apical cytoplasm (e.g., see arrows in Figure 3Aa). The vacuolar portions of a large subset of the GFP-RhoB-associated vesicular elements were labeled by a 5-min pulse of basolaterally internalized fluid-phase marker (Alexa 546-dextran), consistent with GFP-RhoB association with basolateral early endosomes (Figure 3Ac&f). Colocalization was also observed when the fluid-phase marker was internalized from the apical pole of the cell (our unpublished observations). However, colocalization was not observed when the 5-min pulse of basolaterally-internalized fluid-phase marker was chased into late endosomes by an additional 40 min incubation at 37˚C (Figure 3B).

Finally, we examined if there was any colocalization between GFP-labeled vesicular elements and the Golgi. The latter was labeled by the apical addition of BODIPY-ceramide-Texas Red for 60 min at 20˚C followed by a 2-h chase at the same temperature (Figure 3C) (31). There was little observable colocalization between GFP-

labeled vesicular elements and the Golgi complex of living MDCK cells (Figure 3Cc). However, if the cells were warmed to 37˚C, which allows lipid to exit the Golgi, significant colocalization was observed (our unpublished observations). Like endogenous RhoB, GFP-RhoB was localized in part to basolateral early endosomes, but to a lesser degree with late endosomes or with the Golgi.

*Expression of RhoBN19, RhoBV14, and RhoBWT in MDCK cells* - To further examine the cellular distribution of RhoB, we generated stable MDCK cell lines that expressed myc-tagged versions of RhoBWT, RhoBV14, or RhoBN19 in a tetracycline-repressible manner. The dominant active mutant RhoBV14 is locked in its GTP-bound state and is likely to constitutively activate pathways regulated by RhoB, while dominant negative Rho GTPase mutants like RhoBN19 are thought to bind avidly to the guanine nucleotide exchange factors, thereby preventing activation of the endogenous protein (32). These cells also stably express the pIgR. When RhoBN19, RhoBV14, or RhoBWT-expressing cells were cultured in the absence of DC for 48 h, expression of RhoB was observed (Figure 4). No expression was observed in the presence of DC. The level of wild-type and mutant RhoB expression relative to that of endogenous RhoB (measured in cells grown in the presence of DC) was quantified by immunoprecipitation from $^{35}$S-labeled cell lysates. We observed ~43-fold greater expression of RhoBN19, and ~48-fold greater expression for RhoBV14 and RhoBWT, when compared to endogenous RhoB.

Like endogenous RhoB, RhoBWT was associated with vesicular structures that colocalized in part with Tf but only showed a small degree of overlap with giantin, and was associated with large vesicular structures in the apical region of the cells that were positive for the EEA1 (our unpublished observations). RhoBN19 shared a similar distribution to endogenous RhoB. It was localized to the lateral cell surface and was also associated with vesicles along the lateral membranes and in the apical cytoplasm (Figure 5Aa-c). RhoBN19-associated vesicular structures colocalized with Tf (Figure 5Aa-c), and to some degree with the Golgi marker giantin (Figure 5Ag-i), but less so with the M6PR (Figure 5Ad-f). RhoBV14 was associated with vesicles that colocalized with Tf and the M6PR (Figure 5Ba-c & 5Bd-f), and to some extent with giantin (Figure 5Bg-i). Expression of RhoBV14 increased significantly the degree of colocalization between EEA1 and the M6PR (our unpublished observations). These EEA1- and M6PR-positive endosomes were accessible to a 5 min pulse of Tf, indicating they were early endosomes (our unpublished observations). Additionally, the normal ribbon-like distribution of the Golgi resident protein giantin was disrupted by RhoBV14 expression, and giantin in these cells was observed in small vesicles dispersed through out the cytoplasm of the cell (Figure 5Bg-i). Overall, our data indicates that endogenous RhoB, GFP-RhoB, and mutant RhoB are all localized in part to early endosomes of MDCK cells.

*Postendocytic traffic is altered by mutant RhoB expression* - The localization of RhoB to early endosomes prompted us to explore whether RhoB was involved in the regulation of cargo transport through the early endosomal system. In preliminary experiments we observed that expression of RhoBV14, but not RhoBN19, resulted in altered tight junction staining and decreased trans-epithelial resistance (+DC, 306 ± 46 $\Omega$*cm$^2$; -DC, 92 ± 9 $\Omega$*cm$^2$). Because the assays used in these studies measure the release of ligand into the apical and basolateral compartments of the Transwell, we measured whether RhoBV14 expression altered the paracellular flux of [$^{125}$I]IgA and [$^{125}$I]Tf across the cell monolayer. However, we found that less than 1% of apically-added [$^{125I}$]IgA or [$^{125}$I]Tf appeared in the basolateral compartments of RhoBV14-expressing cells after 60 min at 37°C, an increase that would not significantly alter the outcome of the postendocytic fate assays described below.

RhoB is known to modulate EGF transit in other cell types (2,4,12), so we first measured the fate of basolaterally internalized [$^{125}$I]EGF. In control cells, ~55% of this ligand was degraded after 2 h (Figure 6A). RhoBN19 expression generally had no measurable effect on the kinetics of [$^{125}$I]EGF degradation, however, the there was a small, but significant increase in degradation after 2 h (Figure 6A). In RhoBV14-expressing cells, [$^{125}$I]EGF degradation was slowed by ~47%, whereas in RhoBWT-expressing cells the kinetics

of [$^{125}$I]EGF degradation were significantly slowed but the absolute amount of [$^{125}$I]EGF degraded over 2 h differed from control values by only a small amount (Figure 6B&C). The amount of [$^{125}$I]EGF released from the apical surface of the cells (i.e. transcytosed) was significantly increased by ~40-50% in RhoBV14 and RhoBWT-expressing cells (Table I). The pool of [$^{125}$I]EGF that recycled to the basolateral surface of the cell was significantly increased in cells expressing RhoBV14. Conversely, EGF recycling was significantly decreased in cells expressing RhoBN19 (Table I).

As a marker of the basolateral recycling pathway we followed the fate of [$^{125}$I]Tf. The kinetics and absolute amount of [$^{125}$I]Tf recycled were unaffected by expression of RhoBN19 (Figure 6D). In contrast, expression of RhoBWT or RhoBV14 caused a significant decrease in [$^{125}$I]Tf recycling (Figure 6E&F). Although the amount of apical Tf release is typically < 10% of total we observed an ~50% increase in the amount of [$^{125}$I]Tf released from the apical pole of cells expressing RhoBV14, while expression of RhoBN19 decreased [$^{125}$I]Tf transcytosis by ~47% (Table I).

We used apically internalized [$^{125}$I]IgA as a marker of the apical recycling pathway. The pIgR and its ligand IgA move by transcytosis from basolateral early endosomes to common recycling endosomes, to apical recycling endosomes, and finally to the apical pole of the cell where the receptor is cleaved, releasing the soluble ligand-binding portion of the receptor (i.e., secretory component) and associated ligand into the apical medium (33). However, a significant fraction of the receptor escapes cleavage and can be internalized from the apical cell surface where it recycles to the apical membrane (19). While expression of RhoBN19 did not affect the kinetics or extent of apical recycling of IgA (Figure 6G), expression of RhoBV14 or RhoBWT slowed the kinetics of this process and decreased the amount of [$^{125}$I]IgA recycled to the apical surface (Figure 6H&I). While the amount of apical-to-basolateral transcytosis of apically internalized IgA is small (on the order of ~5%), RhoBV14 expression significantly increased apical-to-basolateral transcytosis by ~36% and RhoBN19 expression significantly decreased apical-to-basolateral transcytosis by ~40% (Table I).

We also determined the effect of RhoB mutant expression on the fate of basolaterally internalized [$^{125}$I]IgA. Interestingly, expression of RhoBN19 resulted in a significant increase in the rate of IgA transcytosis (Figure 6J), while expression of RhoBV14 or RhoBWT had the opposite effect (Figure 6K&L). Expression of RhoBV14 or RhoBWT significantly slowed the rate of [$^{125}$I]IgA transport and decreased the absolute amount of transcytosis by ~35%. Whereas RhoBN19 expression stimulated [$^{125}$I]IgA transcytosis, it significantly inhibited [$^{125}$I]IgA recycling to the basolateral surface, and the expression of RhoBV14 or RhoBWT significantly stimulated basolateral recycling of [$^{125}$I]IgA (Table I).

Taken together the above data provide further evidence that RhoB modulates endosomal traffic. Of particular note is that RhoBN19 and RhoBV14 differentially affected a select subset of trafficking pathways, including basolateral-to-apical transcytosis of pIgR-IgA complexes.

*RhoB acts at an early step in the transcytotic pathway* - The differential effects of RhoBN19 and RhoBV14 expression on IgA transcytosis prompted us to explore further the particular transport step(s) that may be modulated by RhoB. We initially tested whether expression of mutant RhoB had any effect on the rate of clathrin-dependent endocytosis of [$^{125}$I]IgA ligand internalized from either the apical nor the basolateral surface of the cell. However, we found that mutant RhoB expression had no effect on the rate of IgA endocytosis (our unpublished observations).

We used a previously-described density shift assay that measures the movement of IgA from basolateral early endosomes to apical endosomes that are accessible to an apically-internalized membrane marker, WGA-HRP (18). The WGA-HRP was internalized from the apical cell surface for 10 min at 37˚C and [$^{125}$I]gA was co-internalized basolaterally for the last 2.5 or 5 min. Residual ligand was removed from the cell surface, and the cells were treated with diaminobenzidine and $H_2O_2$ to cross-link [$^{125}$I]IgA present in the WGA-HRP–filled apical endosomes into a dense, detergent-insoluble complex that following cell lysis in detergent, could be recovered by centrifugation. Expression of

RhoBN19 had a kinetic effect on delivery of [$^{125}$I]IgA to apical endosomal compartments. A significant stimulation (~2.8-fold increase) was observed at 2.5 min, but no effect was observed after 5 min (Figure 7A). In contrast, in RhoBV14-expressing cells the amount of [$^{125}$I]IgA found in the apical endosomes was significantly decreased by ~42% at 2.5 min and by 30% at 5 min (Figure 7B). These results indicated that RhoB modulated IgA transcytosis at an early step, possibly involving transit of pIgR-IgA complex from basolateral endosomes to more apical compartments.

*RhoB modulates the exit of cargo from basolateral early endosomes* - In the assay described above, movement of pIgR-IgA between basolateral and apical endosomes depends on several events including vesicle formation and fission, vesicle transport, and vesicle fusion. To define further the site of action of RhoB, we measured release of IgA-containing transport vesicles from basolateral early endosomes using a permeabilized cell system that reconstitutes this event (23).

[$^{125}$I]IgA was internalized at 18.5˚C for 25 min to accumulate [$^{125}$I]IgA in basolateral early endosomes of cells not expressing RhoB mutant proteins. Under these conditions, internalized IgA was found in early endosomes positive for endogenous RhoB expression (Figure 8A-C). Following mechanical perforation of the apical cell surface, [$^{125}$I]IgA-containing transport vesicles were released in a cytosol and ATP-dependent manner (Figure 8D). When RhoBN19-containing cytosol was used, a significant (~50%) increase in vesicle release was observed above control incubations (Figure 8D). In contrast, when cytosol from cells expressing RhoBV14 was used, a ~25% reduction in vesicle release was observed (Figure 8E). Although differentially localized in the cell, RhoB shares an almost identical effector binding region to RhoA, a closely-related family member. To confirm that the effects of RhoBN19 were specific, we determined whether cytosol prepared from cells expressing a dominant negative mutant of RhoA, RhoAN19, modulated vesicle release. However, RhoAN19-containing cytosol had no effect on IgA vesicle release (Figure 8F). Western blot analysis confirmed that RhoAN19 cytosol contained ~4 times more mutant Rho protein than cytosol containing RhoBN19 (data not shown), thus ruling out the trivial explanation that the lack of effect was a result of having lesser quantities of RhoAN19 protein. These results confirm that the stimulation in IgA vesicle release was specific for RhoB and was not the result of non-specific reduction in RhoA activation.

*RhoBV14 promotes actin polymerization in MDCK cells* - In non-polarized cells RhoBV14 is reported to promote actin assembly on early endosomes and to stimulate the formation of actin stress fibers (6,7,34). We examined the impact of mutant RhoB expression in MDCK cells. In control cells, grown in the presence of DC, phalloidin staining was found at the apical pole of the cells (data not shown), along the lateral surfaces of the cells (Figure 9Ab & 9Bb), and at the base of the cells where it was associated with bundles of stress fibers (Figure 9Af & 9Bf). This distribution of F-actin was also observed in cells expressing RhoBN19 (Figure 9Ad, h). Surprisingly, we observed almost no phalloidin staining in cells expressing RhoBV14 (Figure 9Bd, h).

Because loss of phalloidin binding can result from actin depolymerization or from the recruitment of actin-binding proteins that alter the confirmation of the actin helix (35,36), we further explored the state of the actin cytoskeleton in RhoBV14 expressing cells. Western blot analysis confirmed that the total pool of actin present in RhoBV14 expressing cells was not significantly different ±DC (Figure 9Ca). We also measured the amount of Triton-soluble G-actin versus Triton-insoluble F-actin in the cells. In cells expressing RhoBV14 the amount of F-actin was higher than in cells grown in the presence of DC (Figure 9Cb), indicating that RhoBV14 promoted actin filament assembly and not disassembly in MDCK cells. This was confirmed by immunofluorescence using an anti-actin antibody (Figure 9D). While some stress fibers were observable in RhoBV14 expressing cells (Figure 9Db, e), they were less apparent in cells grown in the presence of DC (our unpublished observations). Unlike previous reports (6,7), we observed little association of actin with the RhoBV14-positive endocytic structures in the cell (Figure 9Da-c) .

## DISCUSSION

*Intracellular distribution of RhoB* - Despite being the first vertebrate Rho-family GTPase to be identified (37), the localization and functions of RhoB remains an open question. The distribution of RhoB is particularly controversial, with reports that RhoB is localized to Tf- and EEA1-positive endosomes, M6PR-, CD63-, Rab7- and LAMP1-positive late endosomes, the Golgi complex, or the nucleus (3,4,6-10). The controversy may stem, in part, from use of different cell types, and examination of the distribution of overexpressed RhoBWT or mutant RhoB, which our studies demonstrate have significant impact on intracellular traffic and thus marker protein distribution. Using several approaches, including examination of the distribution of the endogenous RhoB protein, we have determined that RhoB is present, in part, on the early endosomes of polarized MDCK cells, where it modulates the dynamics of cargo exit from this compartment. The localization of endogenous RhoB to early endosomes is particularly significant because the distribution of many endogenous Rho GTPases is unknown, and there are few studies in which endogenous Rho GTPases have been localized to endocytic compartments (4,9,18,38).

In contrast to recent observations that RhoB is localized to late endosomes of non-polarized HeLa cells (4) or SYF cells (6), we observed little colocalization of endogenous RhoB, GFP-RhoB, or RhoBN19 with markers of late endosomes in MDCK cells. Consistent with previous reports (3,7), we did observe that overexpressed RhoBWT or RhoBV14 was localized to M6PR-positive compartments and EEA1-positive compartments in MDCK cells. In our analysis we observed that these endosomes were labeled with a short pulse of fluid-phase marker or Tf, indicating that at least a subset of them were early endosomal in nature. Early endosomes are known to be the initial sites of multivesicular body formation (39). Therefore, the previously observed RhoBV14-positive multivesicular bodies (8) may in fact reflect trapping of late endosomal cargo and associated vesicular elements in early endosomal compartments. Alternatively, they could result from the fusion of late endosomal content with early endosomes, a possibility that was not directly examined in our studies.

We only observed a small degree of colocalization of endogenous RhoB with recycling endosomes, and we did not observe significant colocalization of endogenous RhoB with the Golgi complex or nucleus. Our analysis of the distribution of RhoB-GFP contrasts with a previous study that localized RhoB to the Golgi complex of MDCK cells (9), and may reflect differences in the protocols used to label this organelle. Michaelson *et al*. internalized BODIPY-ceramide Texas Red at 37˚C for 30 min (9). At this temperature the lipid marker labels both Golgi complex and endosomes, in part because the lipid probe can exit the Golgi complex and recycle at the plasma membrane (40). In contrast, the conditions used in this study (1 h pulse at 20˚C followed by a 2 h chase at 20˚ C) prevent lipid exit from the Golgi (31). We did observe that RhoBN19 and RhoBV14 colocalized to some degree with giantin, and that the distribution of the Golgi apparatus was significantly altered in cells expressing RhoBV14. Therefore, it is possible that activation of RhoB is associated with changes in Golgi structure or function, or that there is a dynamic pool of RhoB that cycles between endosomes and the Golgi, and this pool was missed in our analysis. There was a significant fraction of RhoB in vesicular structures that did not colocalize with EEA1, Tf, Rab11, M6PR, giantin, or furin. These vesicular elements may represent transport intermediates trafficking between the plasma membrane, early endosomes, and other intracellular compartments

*Modulation of endocytic traffic by RhoB and other Rho family GTPases* - An additional significant finding of our study is that RhoB regulates the dynamics of protein exit from early endosomes in MDCK cells and not from late endosomes as previously described (4). Previous studies examined EGF traffic in cells overexpressing RhoBWT or dominant active mutants of RhoB (4,12). Significantly, dominant negative RhoB had no effect on EGF receptor localization or degradation in these previous studies (12). In our analysis we observed that expression of RhoB mutants modulated the traffic of several ligands whose transport involves initial passage through early endosomes: RhoBV14 expression altered the

kinetics of EGF degradation and basolateral recycling of Tf, inhibited basolateral-to-apical transcytosis of IgA, and to a lesser extent decreased apical recycling of IgA. In contrast, expression of RhoBN19 stimulated basolateral-to-apical transcytosis of IgA, indicating that the basal rate of IgA transcytosis is dependent on the activation state of endogenous RhoB. Other pathways affected by RhoBN19 expression included basolateral recycling of EGF, basolateral-to-apical transcytosis of Tf, apical-to-basolateral transcytosis of IgA and basolateral recycling of basolaterally-internalized IgA. The opposing effects of mutant RhoB expression on transcytosis of IgA and Tf have been noted in our previous studies for other GTPases (16,18), and likely reflects differences in the mechanism of how these two pathways are regulated.

The magnitude of the above effects were similar to numerous other reports that have examined the effects of Rab and Rho family GTPases on endocytic traffic (16,18,41-43). Consistent with the hypothesis that RhoB modulates the exit of cargo from early endosomes, we observed that cytosol containing RhoBN19 significantly stimulated vesicle release of IgA from early endosomes in a permeabilized cell system, while RhoBV14 had the opposite effect. Although we cannot rule out that RhoB regulates other forms of internalization or other transport steps in the endocytic system, this is the first report showing that the budding of vesicles from the early endosomes is modulated by RhoB.

In addition to RhoB, multiple Rho family GTPases including Cdc42, Rac1, and RhoA regulate the transcytotic pathway (16,18,44). The first step in this pathway, endocytosis at the basolateral cell surface, was stimulated by expression of dominant negative Rac1N17, but inhibited by expression of dominant negative RhoAN19 (18,44). In contrast, expression of either dominant negative Cdc42N17 (16), or RhoBN19 had no effect. The subsequent movement of endocytosed IgA-pIgR complexes from basolateral to apical endosomes, did not appear to be regulated by Cdc42 or Rac1, but was the apparent target of both RhoA and RhoB (18). However, the mechanism by which RhoA and RhoB modulates this step is likely to be distinct as expression of dominant negative RhoBN19 (or addition of RhoBN19 to a permeabilized cell assay) stimulated IgA transcytosis, while expression of RhoAN19 or addition of this protein to the permeabilized cell assay was without effect (18). Furthermore, RhoA was localized to a subset of endosomes at the very base of the cells that appeared to be associated with stress fibers, and expression of RhoAV14 caused IgA to accumulate in this population of basal endosomes (18). In contrast, RhoB localized to basolateral endosomes found subjacent to the entire basal-lateral surface of the cell. A final step in the transcytotic pathway is movement between different populations of recycling endosomes and the apical cell surface (33). Expression of dominant active Rac1 or Cdc42 was associated with the trapping of IgA cargo in these recycling endosomes (16,44). No such structure was formed in cells expressing mutant RhoA or RhoB, and expression of dominant negative Cdc42N17 inhibited IgA transcytosis (16). Perhaps reflecting the complexity of the transcytotic pathway, multiple members of the Rho family regulate distinct trafficking steps during IgA transcytosis.

*The function of RhoB* - How RhoB modulates exit of cargo from endosomes remains to be defined. Recent studies have shown that RhoBV14 promotes actin assembly on endosomal membranes, possibly through modulation of Scar1, mDia2, and mDia1 activity (6,7). However, in our analysis, we observed little RhoBV14-dependent association of actin with any vesicular compartment in the cell including endosomes. Interestingly, we observed a loss of phalloidin staining in cells expressing RhoBV14, which may reflect changes in the structure of the actin helix that can occurs upon binding of ADF/cofilin and nebulin (35,36). It is possible that RhoBV14 promotes the binding of these proteins to the actin cytoskeleton, thereby modifying the dynamics of actin polymerization/de-polymerization inside the cell. It was previously shown that treatment with the actin disrupting agent cytochalasin D significantly slowed IgA transcytosis (21), that treatment with the actin depolymerizing drug latrunculin B decreased basolateral recycling of Tf while increasing its transcytosis (45), and that delivery to lysosomes is dependent on actin (46). As such, the effects of endocytic traffic we observed in cells expressing RhoBV14 may stem,

in part, from RhoBV14-dependent alterations in the actin cytoskeleton.

In MDCK cells, RhoBV14 does not appear to act by stimulating the activity of its downstream effectors ROCK or mDia1. Consistent with previous studies (7,12), we observed that the ROCK inhibitors Y-27632 or H-1152 did not block the effects of RhoBV14 on postendocytic traffic (our unpublished observations). Moreover, we have generated stable MDCK cell lines that express RhoBV14Y37, a mutant that does not interact with any known RhoB effectors and RhoBV14A39, a mutant that is reported to not interact with ROCK, Rhophilin, Kinectin, Citron or PRK1 but still binds to mDia (47,48). Expression of either one of these mutants largely blocked the inhibitory effects of RhoBV14 on postendocytic traffic, suggesting that mDia does not act downstream of RhoB to regulate these pathways (our unpublished observations). Other known effectors of RhoB include PRK1 and p76RBE (11,12,49), but a role for these proteins in polarized traffic has not been assessed.

How, then, does RhoB modulate traffic through early endosomes? One possibility is that ligand binding to cognate receptors stimulates activation of RhoB either at the plasma membrane or *en route* to or within early endosomes. For example, IgA binding is known to activate secondary messenger cascades that modulate the rate of IgA transcytosis (33), and RhoB can be activated within a few minutes of EGF binding to its receptor (50). In its active, GTP-bound state RhoB could act to slow the exit of cargo from the early endosome, in part, by modulating the activity of downstream effectors that would stabilize cargo in the endosome. Alternatively, RhoBV14 could act by modulating actin dynamics at or near the surface of the early endosome. Such slowing would allow signaling events to propagate and/or terminate. Upon eventual GTP hydrolysis, the disengagement of RhoB effectors and possible cessation of actin turnover would provide a permissive environment for cargo exit from the endosome. While the details of RhoB action remain to be described, our analysis indicates that it is an important regulator of early endocytic traffic in polarized MDCK cells.

## REFERENCES


1. Etienne-Manneville, S., and Hall, A. (2002) *Nature* **420**, 629-635
2. Qualmann, B., and Mellor, H. (2003) *Biochem. J.* **371**, 233-241
3. Adamson, P., Paterson, H. F., and Hall, A. (1992) *J. Cell Biol.* **119**, 617-627
4. Wherlock, M., Gampel, A., Futter, C., and Mellor, H. (2004) *J. Cell Sci.* **117**, 3221-3231
5. Kamon, H., Kawabe, T., Kitamura, H., Lee, J., Kamimura, D., Kaisho, T., Akira, S., Iwamatsu, A., Koga, H., Murakami, M., and Hirano, T. (2006) *EMBO J.* **25**, 4108-4119
6. Sandilands, E., Cans, C., Fincham, V. J., Brunton, V. G., Mellor, H., Prendergast, G. C., Norman, J. C., Superti-Furga, G., and Frame, M. C. (2004) *Dev. Cell* **7**, 855-869
7. Fernandez-Borja, M., Janssen, L., Verwoerd, D., Hordijk, P., and Neefjes, J. (2005) *J. Cell Sci.* **118**, 2661-2670
8. Robertson, D., Paterson, H. F., Adamson, P., Hall, A., and Monaghan, P. (1995) *J. Histochem. Cytochem.* **43**, 471-480
9. Michaelson, D. M., Silletti, J., Murphy, G., D'Eustachio, P., Rush, M., and Philips, M. R. (2001) *J. Cell Biol.* **152**, 111-126
10. Adini, I., Rabinovitz, I., Sun, J. F., Prendergast, G. C., and Benjamin, L. E. (2003) *Genes Dev.* **17**, 2721-2732
11. Mellor, H., Flynn, P., Nobes, C. D., Hall, A., and Parker, P. J. (1998) *J. Biol. Chem.* **273**, 4811-4814
12. Gampel, A., Parker, P. J., and Mellor, H. (1999) *Curr. Biol.* **9**, 955-958
13. Zhang, J., Zhu, J., Bu, X., Cushion, M., Kinane, T. B., Avraham, H., and Koziel, H. (2005) *Mol. Biol. Cell* **16**, 824-834

14. Linstedt, A. D., and Hauri, H. P. (1993) *Mol. Biol. Cell* **4**, 679-693
15. Apodaca, G., Katz, L. A., and Mostov, K. E. (1994) *J. Cell Biol.* **125**, 67-86
16. Rojas, R., Ruiz, W. G., Leung, S. M., Jou, T. S., and Apodaca, G. (2001) *Mol. Biol. Cell* **12**, 2257-2274
17. Urban, J., Parczyk, K., Leutz, A., Kayne, M., and Kondor-Koch, C. (1987) *J. Cell Biol.* **105**, 2735-2743
18. Leung, S.-M., Rojas, R., Maples, C., Flynn, C., Ruiz, W. G., Jou, T.-S., and Apodaca, G. (1999) *Mol. Biol. Cell* **10**, 4369-4384
19. Breitfeld, P., Casanova, J. E., Harris, J. M., Simister, N. E., and Mostov, K. E. (1989) *Meth. Cell Biol.* **32**, 329-337
20. Maxfield, F. R., and Dunn, K. W. (1990) in *Optical Microscopy for Biology* (Herman, B. a. J., K., ed), pp. 357-371, Wiley-Liss, Inc
21. Maples, C. J., Ruiz, W. G., and Apodaca, G. (1997) *J. Biol. Chem.* **272**, 6741-6751
22. Bomsel, M., Parton, R., Kuznetsov, S. A., Schroer, T. A., and Gruenberg, J. (1990) *Cell* **62**, 719-731
23. Bomsel, M., and Mostov, K. E. (1993) *J. Biol. Chem.* **268**, 25824-25835
24. Minamide, L. S., Painter, W. B., Schevzov, G., Gunning, P., and Bamburg, J. R. (1997) *J. Biol. Chem.* **272**, 8303-8309
25. Bucci, C., Parton, R. G., Mather, I. H., Stunnenberg, H., Simons, K., Hoflack, B., and Zerial, M. (1992) *Cell* **70**, 715-728
26. Kornfeld, S. (1987) *FASEB J.* **1**, 462-468
27. Mu, F.-T., Callaghan, J. M., Steele-Mortimer, O., Stenmark, H., Parton, R. G., Campbell, P. L., McCluskey, J., Yeo, J. P., Tock, E. P. C., and Toh, B.-H. (1995) *J. Biol. Chem.* **270**, 13503-13511
28. Leung, S.-M., Ruiz, W. G., and Apodaca, G. (2000) *Mol. Biol. Cell* **11**
29. Sheff, D. R., Daro, E. A., Hull, M., and Mellman, I. (1999) *J. Cell Biol.* **145**, 123-139
30. Bomsel, M., Prydz, K., Parton, R. G., Gruenberg, J., and Simons, K. (1989) *J. Cell Biol.* **109**, 3243-3258
31. van Meer, G., Stelzer, E. H., Wijnaendts-van-Resandt, R. W., and Simons, K. (1987) *J. Cell Biol.* **105**, 1623-1635
32. Feig, L. A. (1999) *Nat. Cell Biol.* **1**, E25-E27
33. Rojas, R., and Apodaca, G. (2002) *Nat. Rev. Mol. Cell Biol.* **3**, 944-955
34. Aspenström, P., Fransson, A., and Saras, J. (2004) *Biochem. J.* **377**, 327-337
35. McGough, A., Pope, B., Chiu, W., and Weeds, A. (1997) *J. Cell Biol.* **138**, 771-781
36. Ao, X., and Lehrer, S. S. (1995) *J. Cell Sci.* **108**, 3397-3403
37. Madaule, P., and Axel, R. (1985) *Cell* **41**, 31-40
38. de Toledo, M., Senic-Matuglia, F., Salamero, J., Uze, G., Comunale, F., Fort, P., and Blangy, A. (2003) *Mol. Biol. Cell* **14**, 4846-4856
39. Katzmann, D. J., Odorizzi, G., and Emr, S. D. (2002) *Nat. Rev. Mol. Cell Biol.* **3**, 893-905
40. Babia, T., Ledesma, M. D., Saffrich, R., Kok, J. W., Dotti, C. G., and Egea, G. (2001) *Traffic* **2**, 395-405
41. Stenmark, H., Parton, R. G., Steele-Mortimer, O., Lutcke, A., Gruenberg, J., and Zerial, M. (1994) *EMBO J.* **15**, 1287-1296
42. Casanova, J. E., Wang, X., Kumar, R., Bhartur, S. G., Navarre, J., Woodrum, J. E., Altschuler, Y. A., Ray, G. S., and Godenring, J. R. (1999) *Mol. Biol. Cell* **10**, 47-61
43. van IJzendoorn, S. C. D., Tuvim, M. J., Weimbs, T., Dickey, B. F., and Mostov, K. E. (2002) *Dev. Cell* **2**, 219-228
44. Jou, T.-S., Leung, S.-M., Fung, L. M., Ruiz, W. G., Nelson, W. J., and Apodaca, G. (2000) *Mol. Biol. Cell* **11**, 287-304
45. Sheff, D. R., Kroschewski, R., and Mellman, I. (2002) *Mol. Biol. Cell* **13**, 262-275
46. van Deurs, B., Holm, P. K., Kayser, L., and Sandvig, K. (1995) *Eur. J. Cell Biol.* **66**, 309-323
47. Sahai, E., Alberts, A. S., and Treisman, R. (1998) *EMBO J.* **17**, 1350-1361

48. Zeng, P. Y., Rane, N., Du, W., Chintapalli, J., and Prendergast, G. C. (2003) *Oncogene* **22**, 1124-1134
49. Mircescu, H., Steuve, S., Savonet, V., Degraef, C., Mellor, H., Dumont, J. E., Maenhaut, C., and Pirson, I. (2002) *Eur. J. Biochem.* **269**, 6241-6249
50. Gampel, A., and Mellor, H. (2002) *Biochem. J.* **366**, 393-398

## ACKNOWLEDGEMENTS

We thank Carol Kinlough and Paul Poland for providing excellent technical support, and Drs. Linton Traub, Silvia Corvera, and Adam Lindstedt for providing antibodies. This work was supported in part by an equipment grant from Dialysis Clinics Inc., an American Heart Association Postdoctoral Fellowship to CR, an American Heart Association Predoctoral Fellowship to RR, and by grants from the National Institutes of Health to GA (DK-59170 and DK-54425), RJH (DK54787), and KWD (DK-51098).

[4]Abbreviations used in this paper: DC, doxycycline; EEA1, early endosome antigen 1; EGF, epidermal growth factor; GFP, green fluorescent protein; M6PR, cation independent mannose-6-phophate receptor; MDCK, Madin-Darby canine kidney; pIgR, polymeric immunoglobulin receptor; PLD; phospholipase D; TGN, *trans*-Golgi network; Tf, transferrin; WGA, wheat germ agglutinin

## FIGURE LEGENDS

**Figure 1.** Cellular distribution of endogenous RhoB in polarized MDCK cells. The distribution of RhoB alone (A-C), RhoB and Tf (D-F), RhoB and the M6PR (G-I), or RhoB and giantin (J-L) was assessed in fixed and permeabilized filter-grown MDCK cells by indirect immunofluorescence. Shown are merged images (comprised of 3-5 optical sections each) from the apical pole of the cell above the nucleus (A, D, G, & J), along the lateral surface of the cells (B, E, H, & K), or near the base of the cells (C, F, I, & L). Examples of colocalization between endogenous RhoB and Tf (or M6PR) are marked with arrows.

**Figure 2.** Distribution of endogenous RhoB, EEA1 and Rab11 in fixed, polarized MDCK cells. Shown are images (which are the projection of 4 optical sections each) from the apical pole of the cell above the nucleus (A, C, E, G, H, I) or along the lateral surface of the cells (B, D, F). RhoB staining is shown in the left-hand panels (A, B, G), EEA1 staining (C, D) and Rab11 staining (H) are shown in the center panels, and merged images are shown in the right-hand panels. Examples of colocalization between endogenous RhoB and EEA1 are marked with arrows.

**Figure 3.** Localization of GFP-RhoB in live MDCK cells. (A) Alexa-546-dextran was internalized from the basolateral pole of filter-grown GFP-RhoB expressing MDCK cells for 5 min at 37˚C. Examples of Alexa-546-dextran localization to the vacuolar region of GFP-RhoB-positive endosomes are marked with arrows. (B) Following the 5-min pulse of Alexa-546-dextran, the cells were washed and incubated in tracer-free medium for 40 min at 37˚C. (C) BODIPY-Ceramide-Texas Red was internalized from the apical pole of the cell for 1 h at 20˚C followed by a 2 h chase at 20˚C. Shown are merged images (3-5 optical sections each) from the apical pole of the cell above the nucleus (Aa-c, Ba-c, & Ca-c) or along the lateral margins of the cell (Ad-f & Bd-f).

**Figure 4.** Inducible expression of myc-tagged RhoBN19, RhoBV14 and wild-type RhoB in polarized MDCK cells. RhoBN19 cells (N19), RhoBV14 cells (V14), or RhoBWT cells (WT) grown in the presence of DC (+DC) or absence of DC (-DC) were solubilized, the resulting lysates were resolved by SDS-PAGE, and immunoblots were probed with a mouse monoclonal anti-myc antibody.

**Figure 5.** Cellular localization of RhoBN19 and RhoBV14 in polarized MDCK cells. The distribution of RhoBN19 and Tf (Aa-c), RhoBN19 and M6PR (Ad-f), RhoBN19 and giantin (Ag-i), RhoBV14 and Tf (Ba-c), RhoBV14 and M6PR (Bd-f), or RhoBV14 and giantin (Bg-i) was assessed by indirect immunofluorescence and confocal microscopy. Shown are merged images (3-5 optical sections each) from the apical pole of the cell above the nucleus (Aa, d, g & Ba, d, g), along the lateral margin of the cell (Ab, e, h & Bb, e, h), and from the base of the cells (Ac, f, i & Bc, f, i).

**Figure 6.** Postendocytic fate of internalized [$^{125}$I]EGF, [$^{125}$I]Tf, or [$^{125}$I]IgA in cells expressing RhoBN19, RhoBV14, or RhoBWT. RhoBN19 cells (A, D, G & J), RhoBV14 cells (B, E, H, & K), or RhoBWT cells (C, F, I & L) were grown in the presence of DC (+DC) or absence of DC (-DC). Shown is the fraction of basolaterally-internalized [$^{125}$I]EGF that was degraded (A-C), the fraction of basolaterally-internalized [$^{125}$I]Tf that was recycled to the basolateral pole of the cell (D-F), the fraction of apically-internalized [$^{125}$I]IgA that recycled to the apical pole of the cell (G-I), and the fraction of basolaterally-internalized [$^{125}$I]IgA that was released from the apical pole of the cell (transcytosed; J-L). The fraction of degraded [$^{125}$I]Tf or [$^{125}$I]IgA in cells grown in the absence or in the presence of DC was not significantly different. Experiments were repeated three times in triplicate and values are mean ± SEM. *Values were significantly different from control ($p < 0.01$) when analyzed using Student's t-test.

**Figure 7.** Quantification of IgA transport from basolateral to apical endosomes in RhoBN19 (A) and RhoBV14 (B) cells. WGA-HRP was internalized for 10 min from the apical surface of RhoBN19 or RhoBV14 cells, grown in the absence of DC (-DC) or presence of DC (+DC). During the last 2.5 min or 5.0 min of the WGA-HRP internalization, [$^{125}$I]IgA was co-internalized from the basolateral surface of the cell and the degree of colocalization was measured using a modified density-shift assay as described in Experimental Procedures. Experiments were repeated three times in triplicate. Values are averages of the means ± SEM from three separate experiments. *Values were significantly different from control ($p < 0.01$), when analyzed using a non-parametric Mann-Whitney test.

**Figure 8.** Effect of RhoBN19 and RhoBV14 on vesicular IgA-pIgR release from mechanically-perforated MDCK cells. (A-C) Distribution of endogenous RhoB (A), and IgA internalized from the basolateral pole of MDCK cells expressing the pIgR for 25 min at 18.5˚C (B) as assessed by indirect immunofluorescence and confocal microscopy. Shown is an optical section along the lateral margin of the cells. A merged image is shown in panel C and examples of colocalization between RhoB and IgA are indicated with arrows. (D&E) [$^{125}$I]IgA was internalized from the basolateral surface of cells not expressing wild-type or mutant RhoB for 25 min at 18.5˚C and the release of vesicles was measured in the presence of an ATP regenerating system and cytosol from RhoBN19 (D) or RhoBV14 (E) cells grown in the presence of DC (+DC) or absence of DC (-DC). Some reactions lacked the ATP-regenerating system (-ATP) or cytosol (-cytosol). The efficiency of vesicle release was ~45% in the presence of ATP and cytosol from cells grown in the presence of DC. Data are from at least three separate experiments performed in triplicate and values are mean ± SEM. *Values were significantly different from control ($p < 0.01$) when analyzed by a non-parametric Mann-Whitney test. (F) Vesicle release was measured in the presence of cytosol prepared from RhoAN19 cells grown in the presence (+DC) or absence (-DC) of DC.

**Figure 9.** Actin cytoskeleton in RhoBN19 and RhoBV14-expressing MDCK cells. RhoBN19 or RhoBV14 cells were grown in the presence of DC (+DC) or absence of DC (-DC). (A-B) The cellular distribution of RhoBN19 (Aa, c, e, g) and phalloidin-labeled F-actin (Ab, d, f, h) and the distribution of RhoBV14 (Ba, c, e, g) and phalloidin-labeled F-actin (Bb, d, f, h) were assessed by indirect immunofluorescence and confocal microscopy. Shown are merged images (3-5 optical sections each) from the lateral surface of the cell (Aa-d & Ba-d), or near the base of the cells (Ae-h & Be-h). (C) F-Actin content in RhoBV14 grown in the presence or absence of DC. Triton X-100-soluble G-actin and Triton X-100-insoluble F-actin fractions were resolved by SDS-PAGE and immunoblots were probed with a rabbit polyclonal anti-actin antibody. 15 μg of total protein were loaded in each lane. (D) The cellular

distribution of RhoBV14 (Da, d) and actin (Db, e) was assessed by indirect immunofluorescence and confocal microscopy. Actin was detected using an anti-actin antibody. Shown are merged images (3-5 optical sections each) from the apical region of the cell (Da-c), or near the base of the cells (Dd-f).

**Table I. Quantification of postendocytic fate of internalized [$^{125}$I]EGF, [$^{125}$I]Tf, or [$^{125}$I]IgA in cells expressing RhoBN19, RhoBV14, and RhoBWT.** RhoBN19 cells, RhoBV14 cells or RhoBWT cells were grown in the presence of DC or absence of DC. Shown is the percentage increase (+) or decrease (-) of ligand release (relative to control cells grown in the presence of DC) for the following ligands: basolaterally-internalized [$^{125}$I]EGF that was recycled to the basolateral pole of the cell (Bl) or transcytosed and released at the apical pole of the cell (Ap); basolaterally-internalized [$^{125}$I]Tf that transcytosed and released at the apical pole of the cell; apically-internalized [$^{125}$I]IgA that transcytosed and release at the basolateral pole of the cell; and basolaterally-internalized [$^{125}$I]IgA that was recycled and released at the basolateral pole of the cell. Experiments were repeated three times in triplicate and values are mean ± SEM. *Values were significantly different from control ($p < 0.01$) when analyzed using Student's t-test.

| | **RhoBV14** | **RhoBN19** | **RhoBWT** |
|---|---|---|---|
| **EGF recycled (Bl)** | +24.8±0.5* | -16.5±0.5* | -9.4±0.5 |
| **EGF transcytosed (Ap)** | +49.3±0.1* | +10.5±1.1 | +40.7±0.9* |
| **Tf transcytosed (Ap)** | +53.5±0.3* | -46.4±0.5* | +36.3±1.0* |
| **IgA transcytosed (Bl)** | +35.7±0.4* | -40.6±0.2* | -29.2±1.2* |
| **IgA recycled (Bl)** | +35.7±1.1* | -20.9±1.2* | +46.3±0.8* |

Figure 1. Rondanino *et al.*

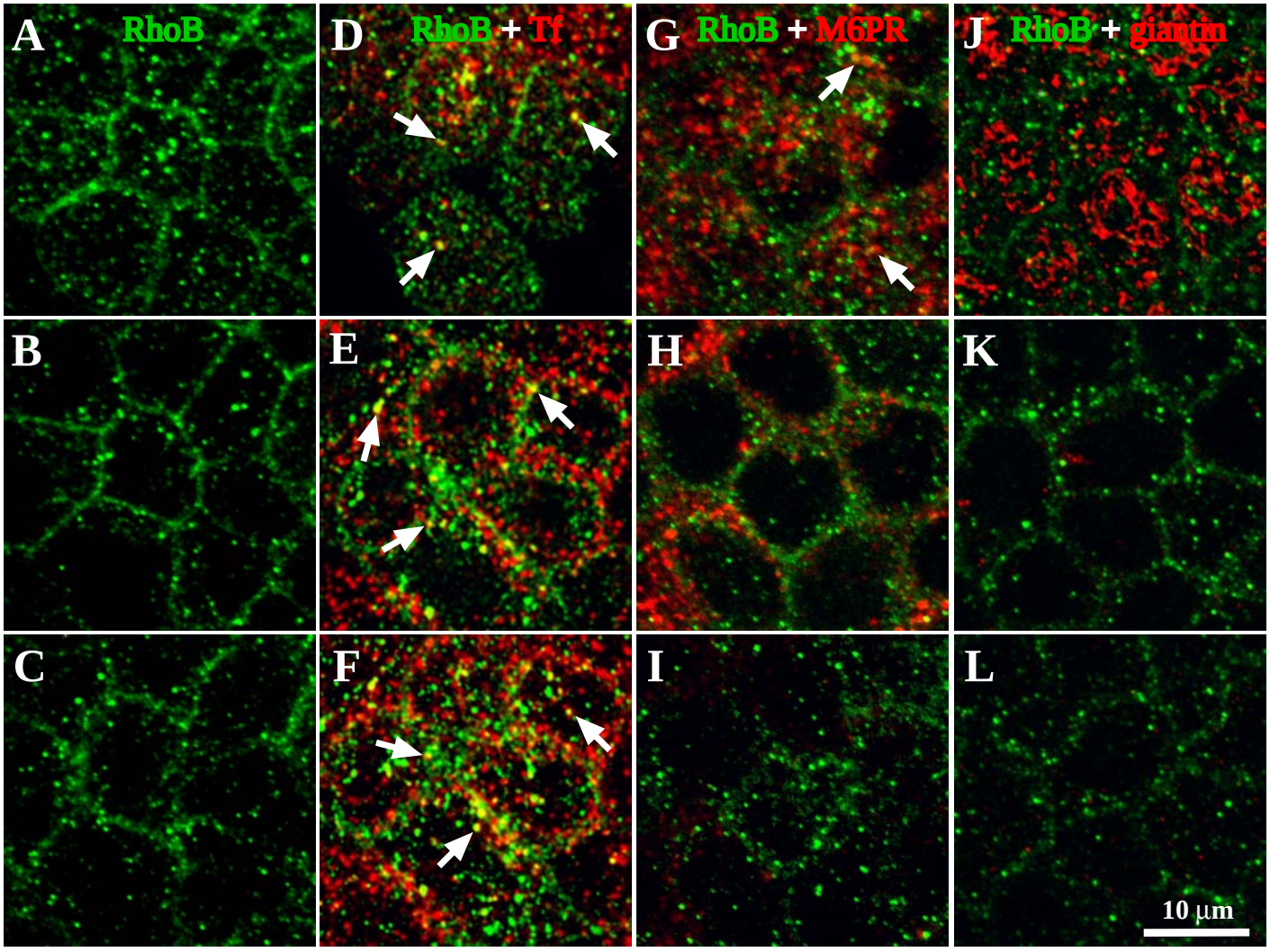

Figure 2. Rondanino *et al.*

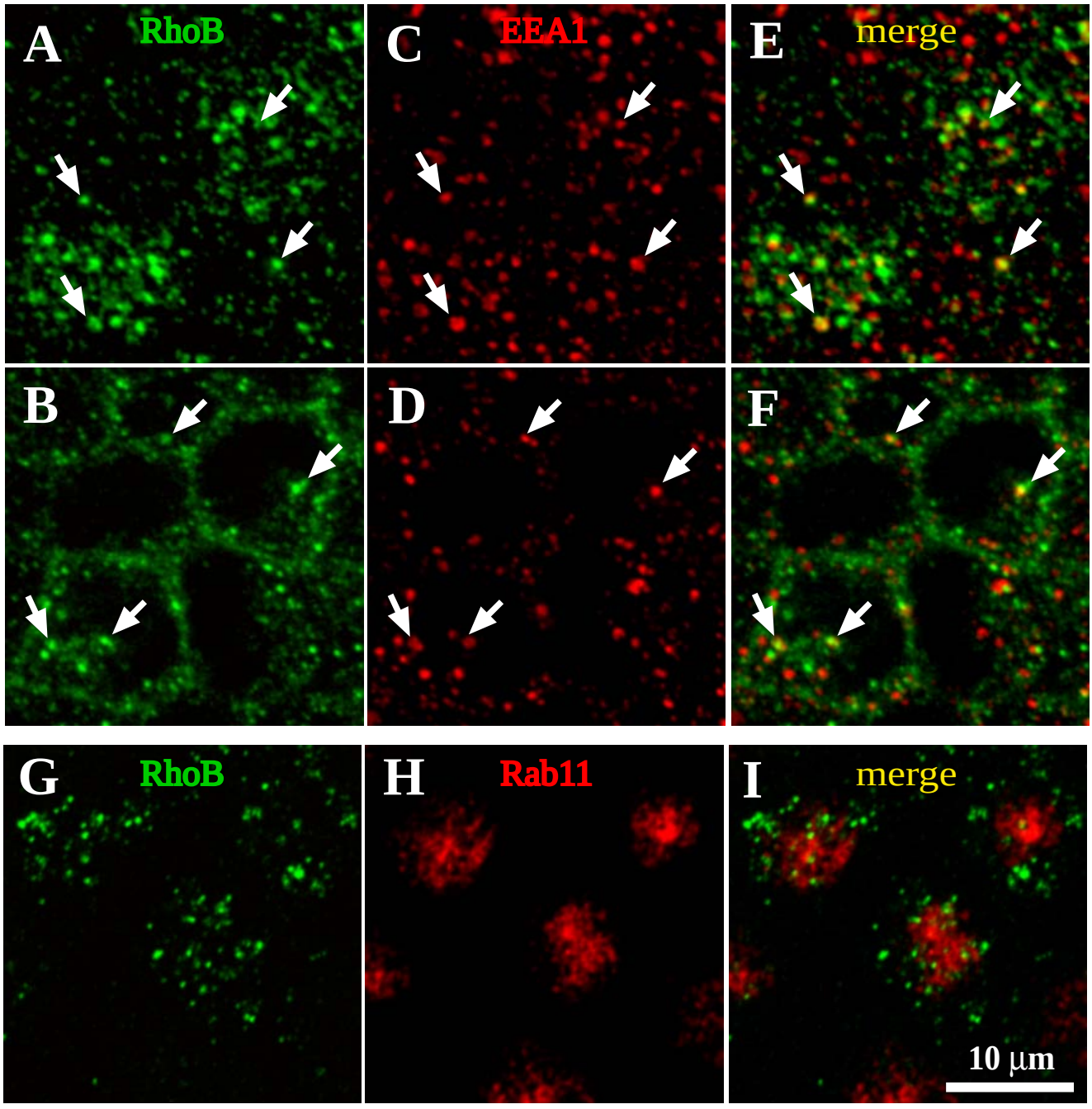

# Figure 3. Rondanino *et al.*

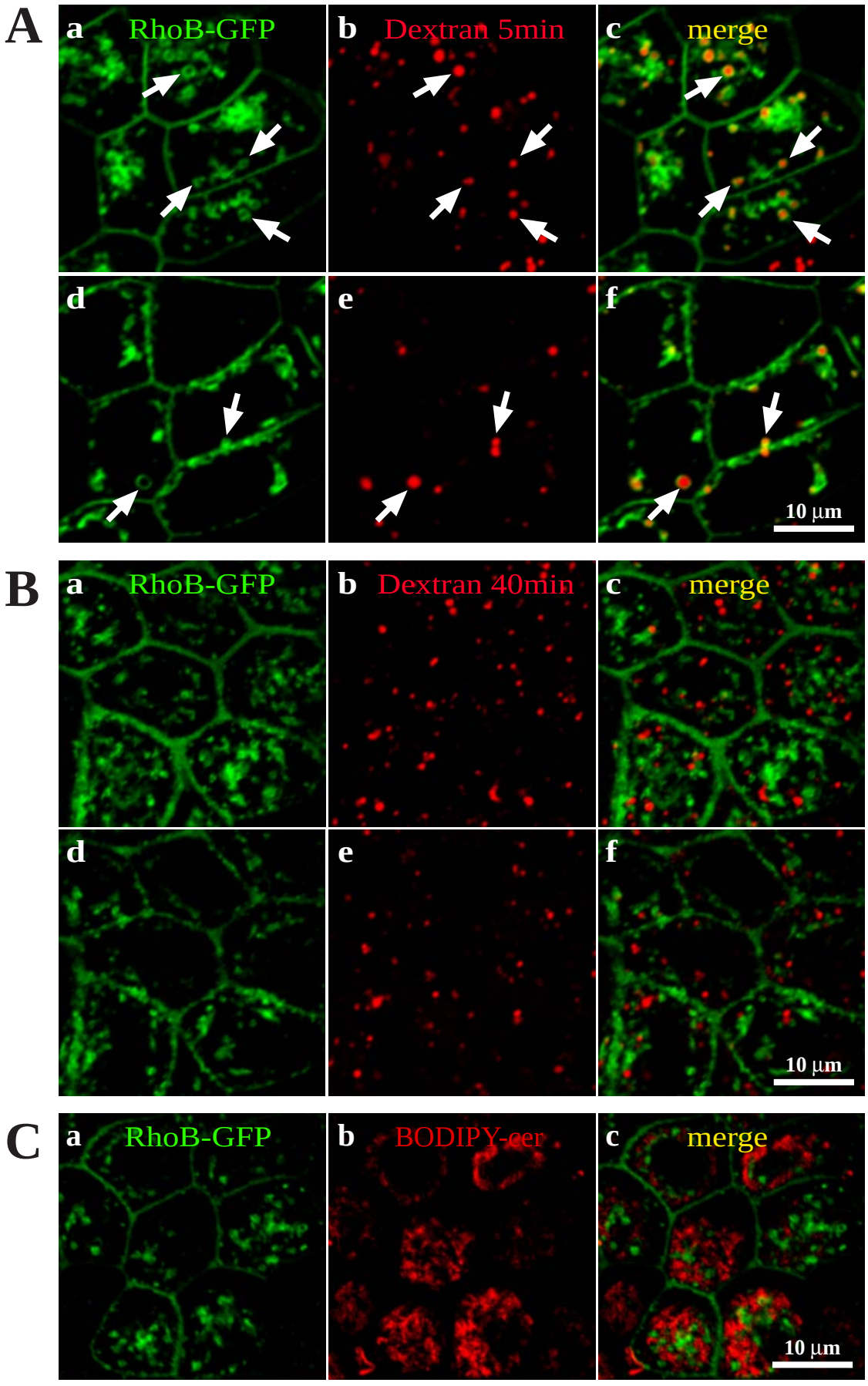

Figure 4. Rondanino *et al.*

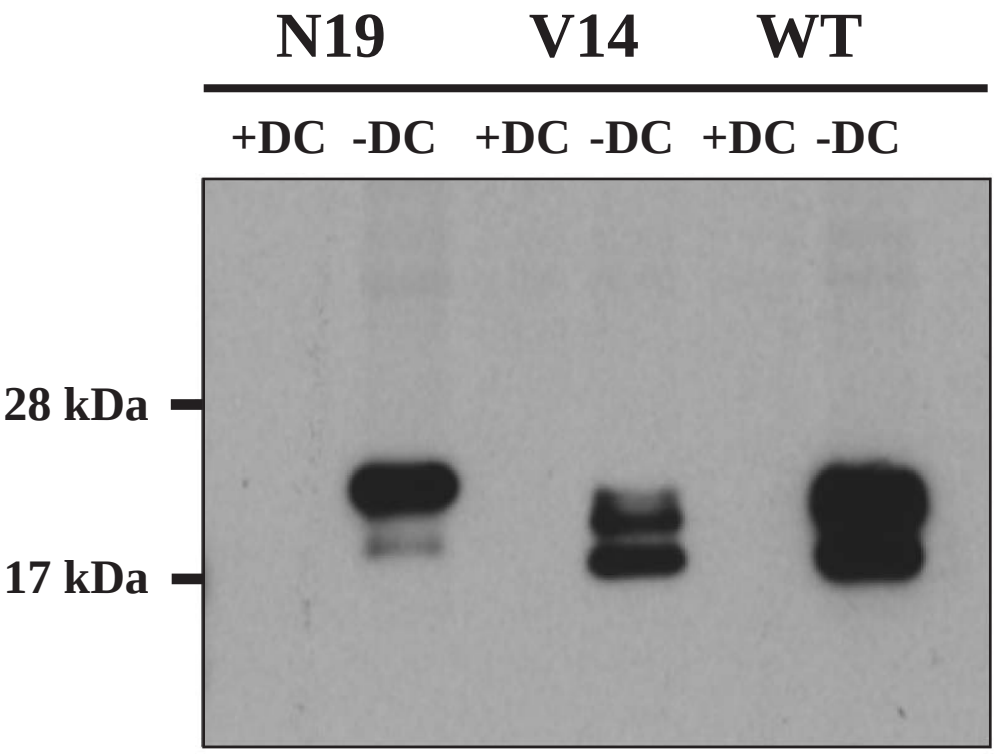

Figure 5. Rondanino *et al.*

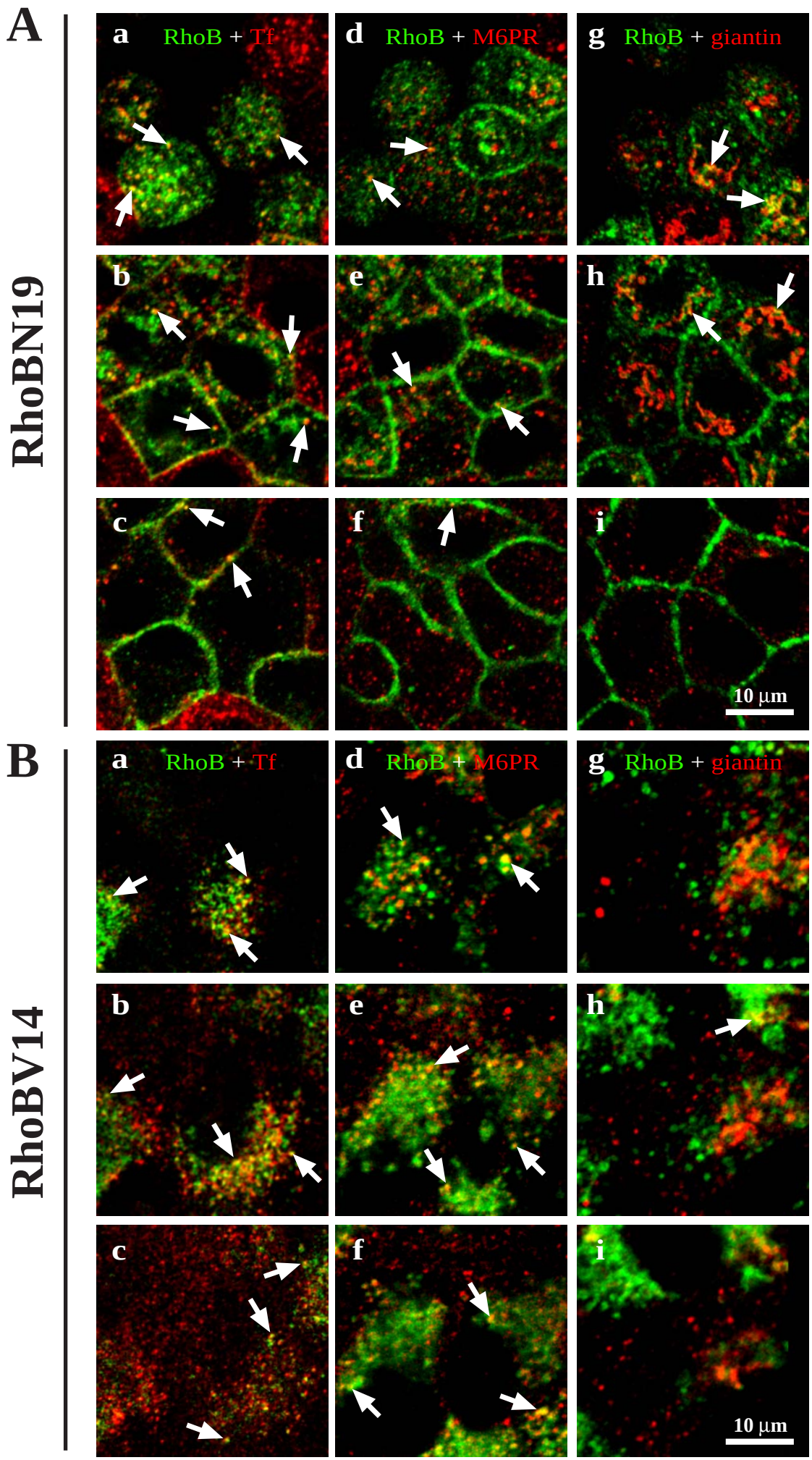

# Figure 6. Rondanino *et al.*

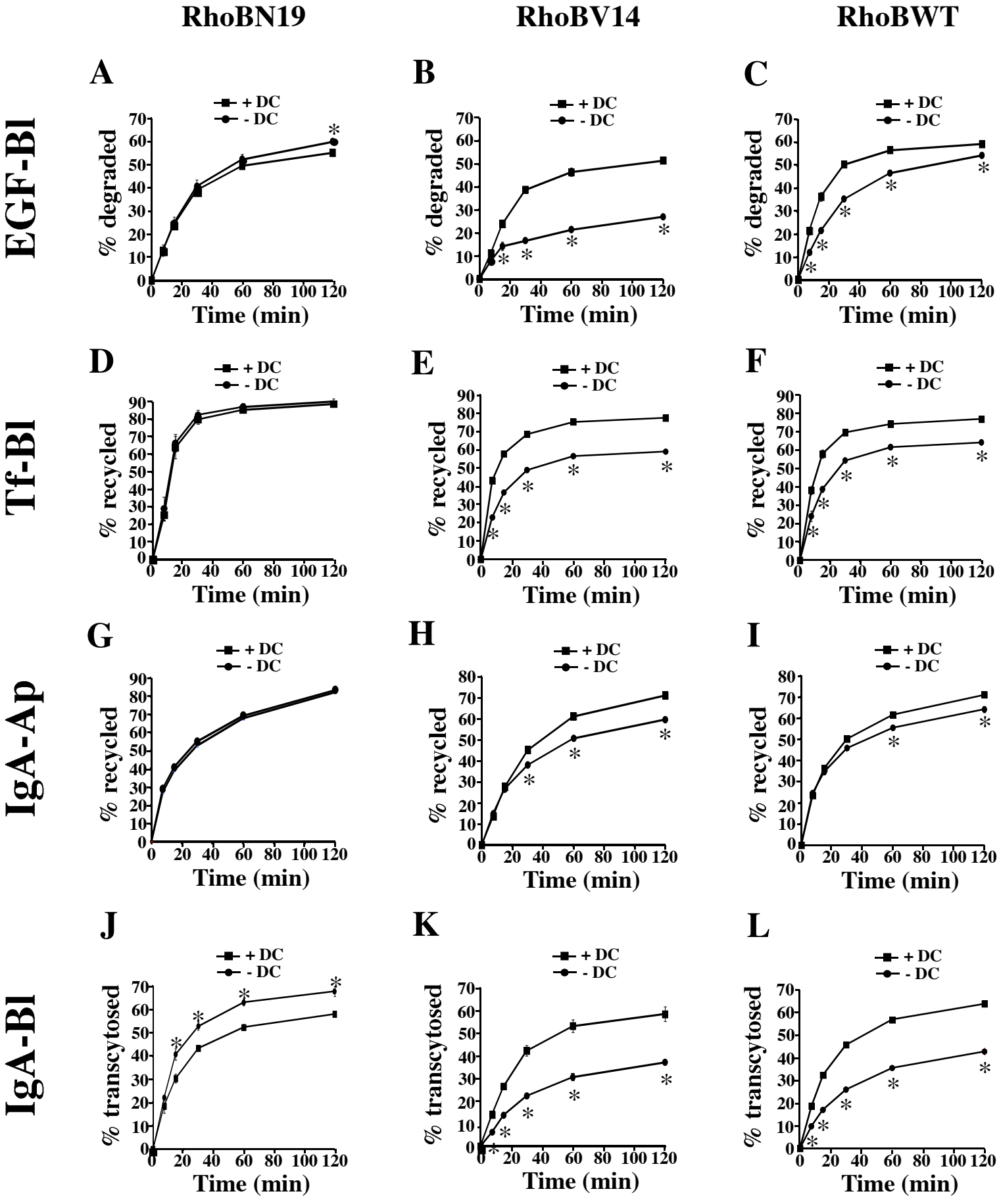

Figure 7. Rondanino *et al.*

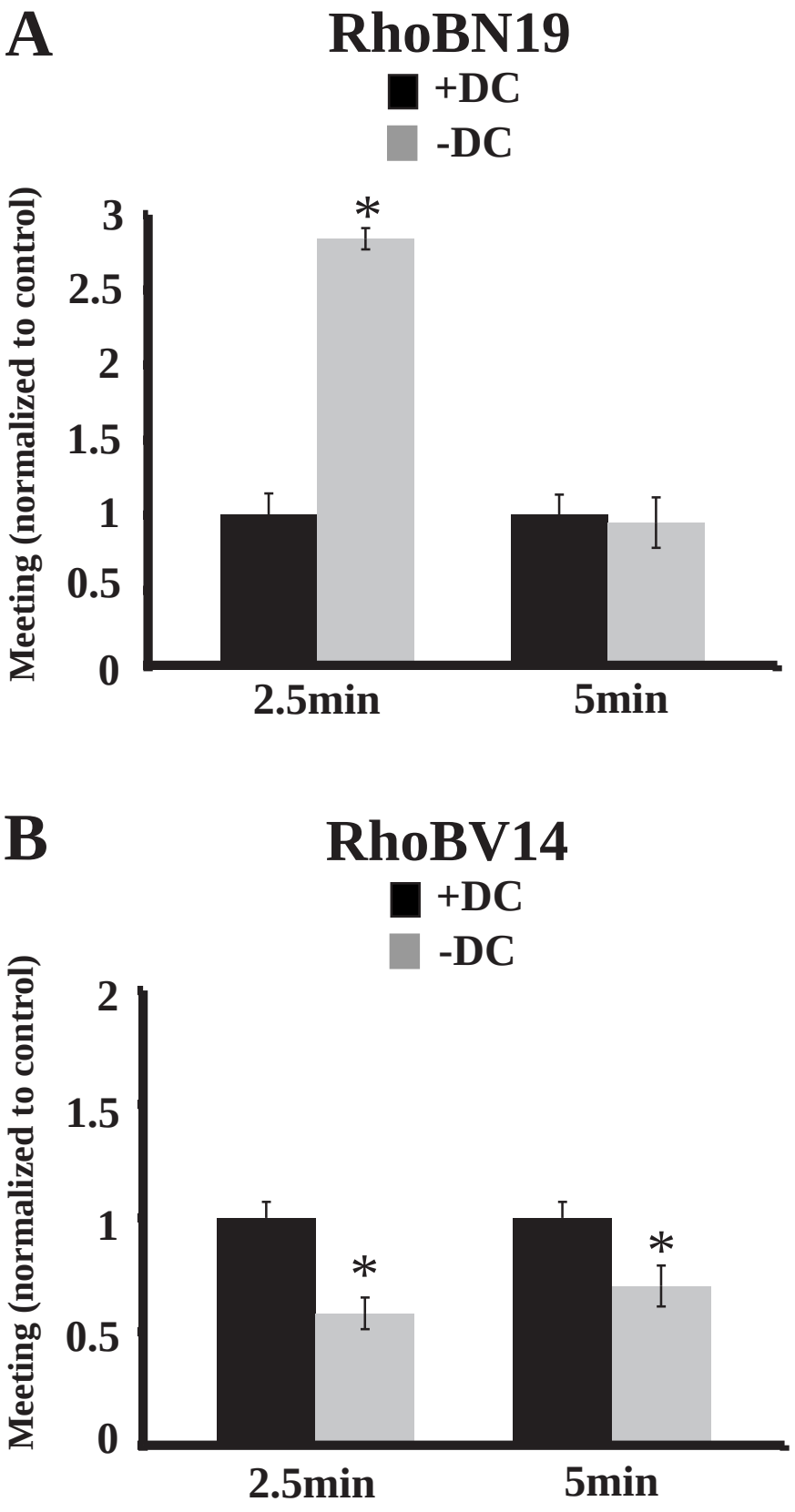

# Figure 8. Rondanino *et al.*

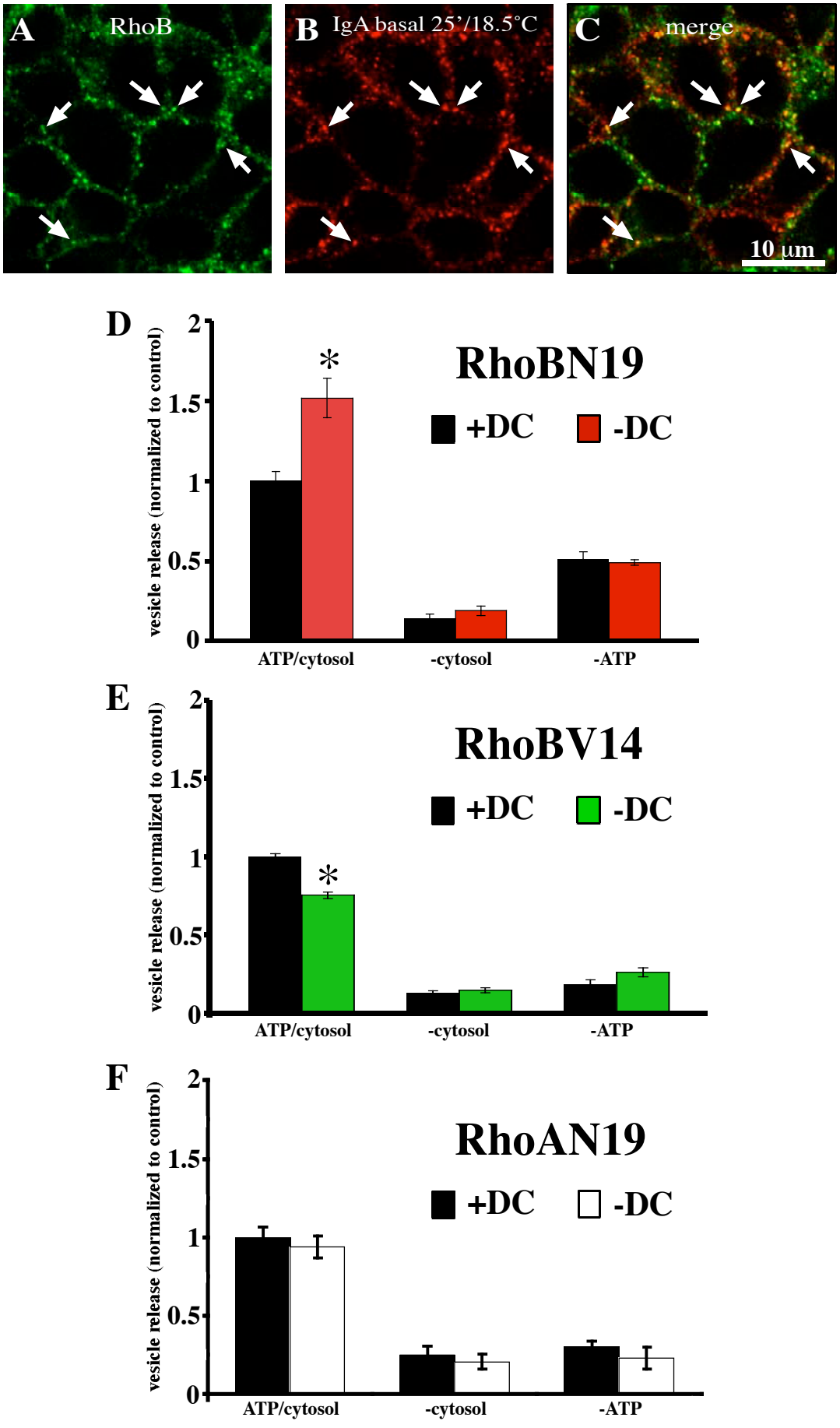

Figure 9. Rondanino *et al.*